

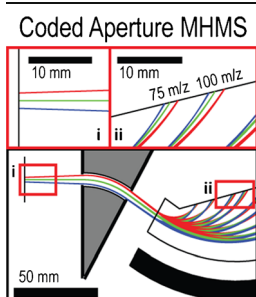
RESEARCH ARTICLE

Compatibility of Spatially Coded Apertures with a Miniature Mattauch-Herzog Mass Spectrograph

Zachary E. Russell,¹ Shane T. DiDona,¹ Jason J. Amsden,¹ Charles B. Parker,¹ Gottfried Kibelka,² Michael E. Gehm,¹ Jeffrey T. Glass¹

¹Department of Electrical and Computer Engineering, Duke University, Durham, NC 27708, USA

²CMS Field Products, OI Analytical, a Xylem brand, College Station, TX 77842-9010, USA



Abstract. In order to minimize losses in signal intensity often present in mass spectrometry miniaturization efforts, we recently applied the principles of spatially coded apertures to magnetic sector mass spectrometry, thereby achieving increases in signal intensity of greater than 10× with no loss in mass resolution Chen et al. (J. Am. Soc. Mass Spectrom. **26**, 1633–1640, 2015), Russell et al. (J. Am. Soc. Mass Spectrom. **26**, 248–256, 2015). In this work, we simulate theoretical compatibility and demonstrate preliminary experimental compatibility of the Mattauch-Herzog mass spectrograph geometry with spatial coding. For the simulation-based theoretical assessment, COMSOL Multiphysics finite element solvers were used to simulate electric and magnetic fields, and a custom particle tracing routine was written in C#

that allowed for calculations of more than 15 million particle trajectory time steps per second. Preliminary experimental results demonstrating compatibility of spatial coding with the Mattauch-Herzog geometry were obtained using a commercial miniature mass spectrograph from OI Analytical/Xylem.

Keywords: Magnetic Sector, Coded aperture, Miniature mass spectrometer, Charged particle optics, Mattauch-Herzog

Received: 18 September 2015/Revised: 6 December 2015/Accepted: 7 December 2015/Published Online: 7 January 2016

Introduction

Mass spectrometers are the gold standard for chemical detection and identification. Sector mass spectrometers in particular are noted for high performance in figures of merit such as mass resolution and detection limit [3, 4]. To achieve such high performance, sector instruments are historically quite large and expensive [5]. Miniaturization of these instruments is useful for the following evolving fields: (1) trace explosive detection and airport security [6, 7], (2) space exploration [8–10], (3) environmental monitoring [11, 12], and (4) point-of-care medical applications [13, 14]. Several groups have demonstrated examples of miniaturized mass spectrometers [15–17]. When miniaturized, these instruments suffer from performance loss in either resolution or signal intensity compared with their full-scale counterparts [18].

Spatially coded apertures have been studied extensively in optical spectroscopy [19] and shown to provide dramatic

improvements in performance, such as increasing signal intensity. Spatial coding techniques were proposed as early as 1970 for mass spectrometry [20] but, to our knowledge, have only recently been demonstrated [1, 2]. The object slit aperture in a simple 90° magnetic sector mass spectrograph similar to Aston's original instrument [21] was replaced with a patterned array of spatially distributed slits. The resulting patterned spectra recorded on an imaging ion detector were reconstructed into traditional mass spectra, demonstrating an increase in signal intensity of more than 10× for a 1D arrays of slits and 3.5× for a 2D array of slits, with no observable loss of resolution [1, 2]. The patterns for these codes were derived from a binary Hadamard code called an S-matrix [22]. The intensity of a spatially coded mass spectrum increases with the order of the coded aperture. Since the increase in signal intensity is proportional to the total open area of a code and the code is roughly 50% opaque, the expected gain of a coded system is $(N + 1)/2$, where N is the order of the coded pattern used. This relationship is described in [1]. Note that the intensity or throughput of the coded spectrum is proportional to the total open area of the pattern, but the resolution is defined by the smallest feature of the code [23].

Zachary E. Russell and Shane T. DiDona contributed equally to this work.

Correspondence to: Jeffrey T. Glass; e-mail: jeff.glass@duke.edu

Double-focusing sector instruments offer substantially improved mass resolving power over the 90° sector design utilized for the preliminary proof of concept development of spatial coding for mass spectrometers [1, 2]. Double-focusing enables simultaneous first order correction of angular and energy dispersion. Spectrographs are mass spectrometers that offer simultaneous analysis of a large mass range projected across a focal plane. Examples of double-focusing mass spectrographs include the Mattauch-Herzog [24], the Bainbridge-Jordan [25], and the Hinterberger-Konig [26]. These geometries employ an electric sector followed by a magnetic sector. Because of its small form factor, which results from the comparatively small sector angles and short drift regions, the Mattauch-Herzog geometry (Figure 1, Table 1) is of particular interest for miniaturized magnetic sector mass spectrometer development. In this paper, we demonstrate the compatibility of coded apertures with the Mattauch-Herzog geometry by using (a) first principles geometric optics transfer matrix calculation, (b) high fidelity finite element field solvers and high particle count charge particle optics simulations, and finally (c) preliminary experimental verification using a commercially available miniature Mattauch-Herzog instrument. We also determine the critical design parameters that enable the use of coded apertures in the Mattauch-Herzog geometry.

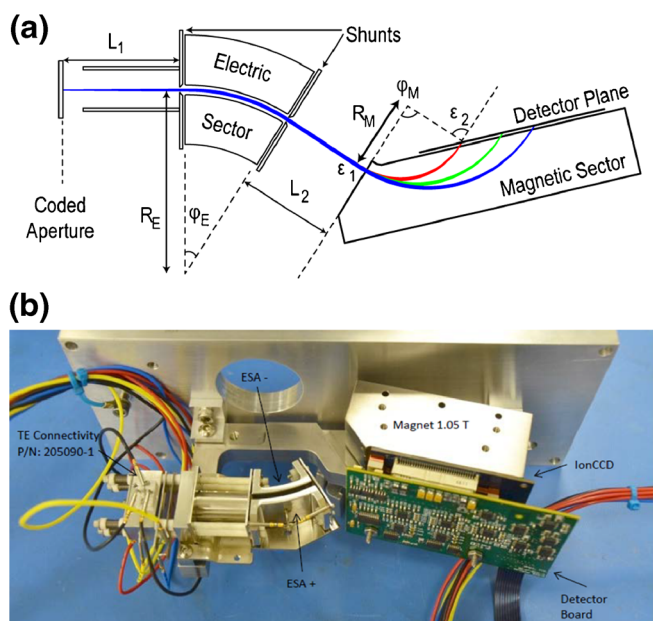


Figure 1. The Mattauch-Herzog mass spectrograph configuration was chosen for this work because of its small form factor. **(a)** This schematic highlights several critical geometric parameters of this design that are important to this study. Additional geometric parameters for this configuration are shown in Table 1, as well as explicit values for the experimental work presented in this manuscript. **(b)** A photograph of the commercially available miniature Mattauch-Herzog platform used in this work (IonCam Product, OI Analytical, a Xylem Brand. College Station, TX). (Image courtesy of OI Analytical, a Xylem Brand)

Simulation of Spatial Aperture Coding in the Mattauch-Herzog Geometry

In this section, we report on methods the two approaches used to simulate spatial coding in a Mattauch-Herzog mass spectrometer. Initial efforts focused on simulations to ensure no fundamental issues existed that inhibited the use of spatial codes in the Mattauch-Herzog geometry and determine potential performance improvements. Transfer matrix calculations were used to determine initial compatibility. For an ideal system, a high fidelity particle tracing simulation method was then used to obtain a more realistic compatibility simulated performance and estimate. In the following section, experimental verification of compatibility was performed using the miniature Mattauch-Herzog mass spectrograph shown in Figure 1 (OI Analytical, a Xylem brand, College Station TX).

Geometric Optics Transfer Matrix Calculation

In order to validate compatibility of this geometry with spatially coded apertures, first order transfer matrix optics calculations were used as an initial model [27]. In the geometric optics approximation, ions are characterized by their positions relative to the optical axis, their angle relative to the optical axis, their energy, and their mass. By successive matrix multiplication (each matrix representing an optical element [19, 28–30]), ions are passed through the system.

This method was discussed by Wollnik [28, 29] and Herzberger [30] for mass spectrometry applications, and Brady [19] for aperture coding applications. The general form

Table 1. Important Geometric Parameters for the Mattauch-Herzog Geometry. Ideal Theoretical Values are Those Inherent to the Mattauch-Herzog Geometry [24]

Symbol	Geometric dimension	Ideal theoretical value	Experimental value
L_1	Aperture to E-sector distance	L_1	35.35 mm
R_E	Electric sector centerline radius	$\sqrt{2}L_1$	50 mm
L_2	E-sector to magnet distance	L_2	20 mm
L_3	Magnet to sensor distance	0	1 mm ^a
R_M	Ion radius in magnetic sector	$\frac{1}{B} \sqrt{\frac{2Vm}{q}}$	25.75 mm ^b
ϕ_E	Geometric angle of electric sector	$\frac{\pi}{4\sqrt{2}}$	31.8°
ϕ_M	Angle ions travel in magnetic sector	$\frac{\pi}{2}$	$\frac{\pi}{2}$
ϵ_1	Magnetic sector entrance angle	0	0
ϵ_2	Magnetic sector exit angle	$-\frac{\pi}{4}$	$-\frac{\pi}{4}$
B	Magnetic field Strength	B	1.05 T
V	Ion accelerating potential	V	800 V

^aThis value deviates from the theoretical value due to detector fabrication constraints

^b R_M for 40 m/z charged particles

of the transfer matrices used for this work was taken from Burgoyne [27] is shown in Eq. (1).

$$\begin{bmatrix} x_f \\ a_f \\ \partial E_f \\ \partial M_f \end{bmatrix} = \begin{bmatrix} (x|x) & (x|a) & (x|\partial E) & (x|\partial M) \\ (a|x) & (a|a) & (a|\partial E) & (a|\partial M) \\ 0 & 0 & 1 & 0 \\ 0 & 0 & 0 & 1 \end{bmatrix} \begin{bmatrix} x_i \\ a_i \\ \partial E_i \\ \partial M_i \end{bmatrix} \quad (1)$$

In this form, the $[4 \times 1]$ element on the left-hand side of Eq. (1) represents the output observed on the detector plane of the spectrometer, the $[4 \times 1]$ element on the right-hand side of Eq. (1) represents the input to the system, and the $[4 \times 4]$ element on the right-hand side of Eq. (1) represents the optics of the mass spectrometer that determine how the input is transformed to the output on the detector. For any system, the output can be determined for any incident particle with a given position x_i , a_i , energy dispersion ∂E_i , and mass dispersion ∂M_i . The $[4 \times 4]$ element representing the spectrometer can be constructed by the multiplication of each discrete lens element in the systems transfer matrix. The MHMS geometry shown in Figure 1 consists of the lens combination shown in Eq. (2), where the individual matrices' meanings are defined in Table 2 and their content is defined in Burgoyne [27].

$$[System] = [D_3][O_2][S_M][O_1][D_2][S][S_E][S][D_1] \quad (2)$$

By substituting the transfer matrix for each lens element [27], the following total system transfer matrix represents the Mattauch-Herzog double-focusing geometry:

$$[System] = \begin{bmatrix} \frac{R_M}{\sqrt{2}L_1} & 0 & 0 & \frac{R_M}{2} \\ -L_1 + L_2 + R_M & -\sqrt{2}L_1 & (-1 + \sqrt{2})L_1 + L_2 + R_M & 0 \\ \sqrt{2}L_1 R_M & \frac{R_M}{0} & \frac{2R_M}{1} & 0 \\ 0 & 0 & 0 & 1 \end{bmatrix} \quad (3)$$

One million ions with energy of 800 ± 8 eV generated from a point source 4 cm behind the aperture were created and transformed by the MHMS transfer matrix in Eq. (3). This mean energy is the same as that used for experimental validation, but the energy spread is larger than that of the real system.

Table 2. Meanings of the Transfer Matrix Symbols. The Content of the Transfer Matrices can be Found in [27]. Each Matrix on the Right Hand Side Represents a System Component or Feature

Matrix symbol	Meaning
$[D_1]$	Drift length 1
$[S]$	Sense matrix
$[S_E]$	Electric sector
$[D_2]$	Drift length 2
$[O_1]$	Magnet entrance angle
$[S_M]$	Magnetic sector
$[O_2]$	Magnet exit angle
$[D_3]$	Drift length 3

Figure 2 shows histograms of the spatial distribution of these ions at the object plane where the coded aperture or slit would be located (Figure 2a), and the predicted output at the detector plane (Figure 2b). The intensity shown on the y-axis in each graph is normalized to the intensity of the pattern at the object image plane of the coded aperture (the object slit plane in traditional systems). The bin size used for the histograms is $24 \mu\text{m}$ and corresponds to the pitch spacing of the commercially available detector used in the experimental portion of this work [31]. The Mattauch-Herzog geometry results in a demagnification of the aperture pattern onto the detector plane, but the structure of the pattern is well preserved, indicating basic stigmatic imaging properties (little or no spatial distortion) of this geometry under this first-order approximation and thus, the MHMS geometry is expected to be compatible with spatial aperture coding.

The matrix algebra and accompanying linearization of the transfer function of the Mattauch-Herzog mass spectrograph do not take into account the fringing fields of the sectors, although there are methods for accounting for fringing fields with an additional lens element [29]. Further, the matrix method is a linear approximation that is not valid for large spatial distributions of ions that are far from the optical axis of the system. Thus, the second method using COMSOL for high fidelity field calculations and a C# program for particle tracing was used to address these limitations.

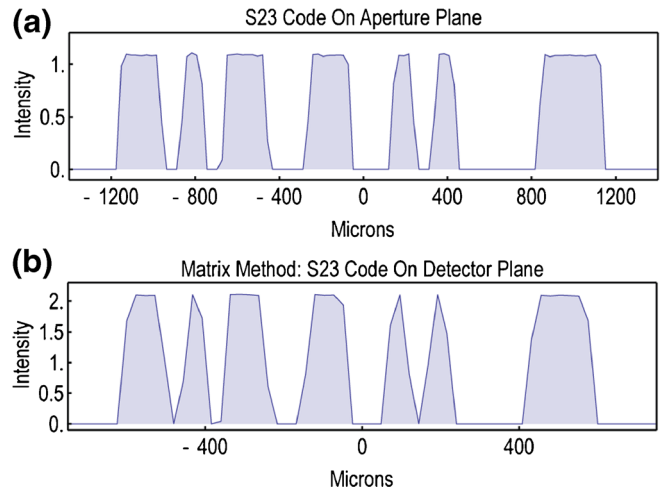


Figure 2. (a) Initial ion distribution across the object plane normalized to the intensity of the pattern at the image plane of the coded aperture. This distribution represents the ions to be passed through the system transfer matrix. (b) Expected ion distribution on the detector plane for Ar^{+1} ($40 m/z$) after passing through the Mattauch-Herzog transfer matrix. Intensity has been normalized to the intensity of the pattern at the image plane of the coded aperture. One million ions were simulated with energy of 800 ± 8 eV from a spherical source 4 cm behind the aperture, and a bin size of $24 \mu\text{m}$ was used for plotting the histograms. We observe the coded aperture pattern is demagnified but remains clearly resolvable on a detector with $24 \mu\text{m}$ pitch spacing, such as the one used for the experimental portion of this work [32]

Particle Tracing Using COMSOL and C#

In order to include the critical effects of fringing fields at the entrance and exit of the electric and magnetic sectors and to remove the constraint imposed by the small angle approximation in the transfer matrix calculation, we built a simulation in the finite element multiphysics simulation program COMSOL (COMSOL, Inc., Burlington, MA USA) and a custom particle tracing program written in C# (Microsoft Visual Studio Professional, Microsoft, Redmond, WA, USA). The COMSOL simulation was used to generate the electric and magnetic fields of the simulated geometries. The generated fields were then imported into a C# program, which calculated ion trajectories with a velocity Verlet algorithm [33] as shown in Figure 3.

The C# program had two functions. First, it generated large numbers of ions with realistic distributions of energy and direction vectors. Second, it passed these ions through the simulated fields of the system. This simulation approach is able to very accurately incorporate fringing fields, which are of critical importance in miniaturized systems because of the large fraction of the ions' total flight path that lies within fringing field regions. This combined approach allowed us to simulate particle trajectories substantially faster than we could have done using COMSOL's particle tracing program. In addition to calculation speed, the C# code evaluated more than 10^6 time

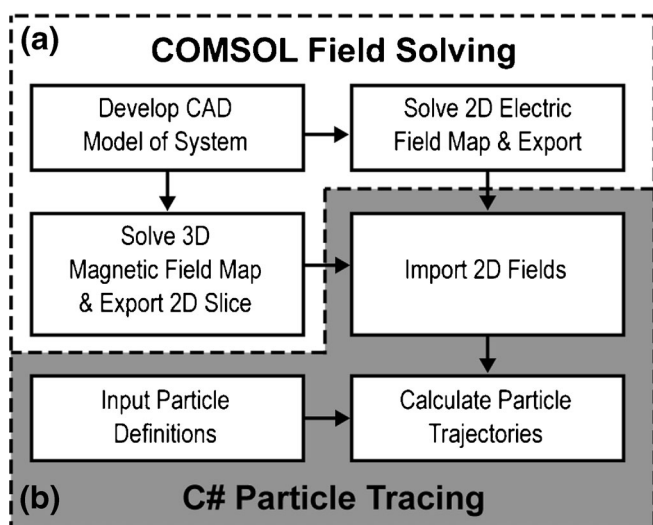


Figure 3. Two simulation approaches were used to verify the compatibility of coded apertures in a MHMS: **(a)** a Gaussian optics transfer matrix calculation, and **(b)** a combined COMSOL/C# particle tracing simulation. Starting from a 3D CAD model of the Mattauch-Herzog geometry, high fidelity COMSOL finite element simulations provided electric and magnetic field maps to be used by our custom C# particle tracer. The C# particle tracer enabled simulation of a statistically significant number of particle trajectories to be calculated quickly, and was used to determine the pattern produced by these particles landing on the detector plane

steps along each ion trajectory. This simulation fidelity is $100\times$ higher than the best we could achieve using the COMSOL particle tracing module on the same workstation, and produced particle trajectories and resulting histogram patterns with much less discretization errors. This approach is limited in that it requires a substantial amount of random access memory to execute with appropriate fidelity, but working in 2D instead of 3D reduces that burden substantially. Note that the magnetic field model requires a 3D simulation to take into account the fringing fields and the effect of the yoke on the fields, so these field calculations were performed in 3D, and then a 2D slice along the midplane of the 3D field profile was exported to the particle trajectory solver. Values of E_x , E_y , and B_z along the midplane of the simulation were recorded with a spatial resolution of $15\ \mu\text{m}$ for use in the particle tracing and are displayed

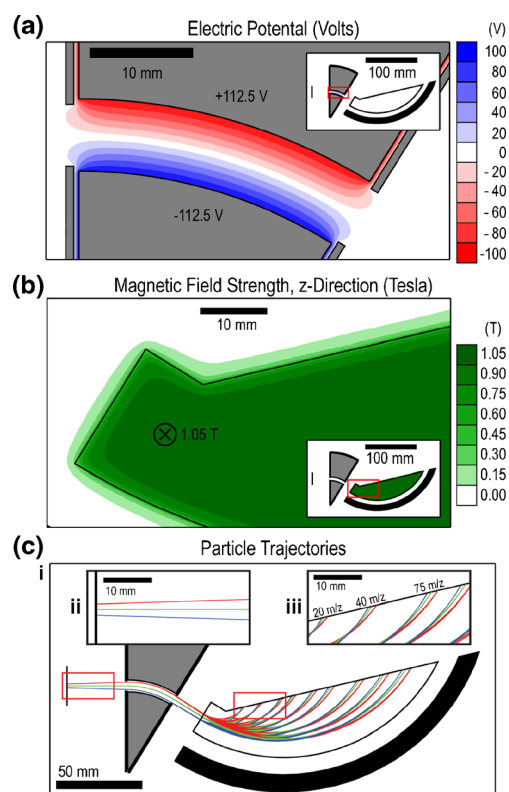


Figure 4. **(a)** The electrical potential map for the Mattauch-Herzog style mass spectrograph used for the particle tracing portion of this work. **(b)** The magnetic field map for the same. **(c)** **(i)** Characteristic particle tracing paths for particles of masses 20, 40, 75, 100, 150, 200, 300, 400, 500 m/z . **(ii)** A zoom in of the spatially distributed ions leaving the coded aperture object plane. The central green paths from particles created on the optical axis, with the upper red and lower blue paths from particles created at $+/- 1150\ \mu\text{m}$. **(iii)** Close up of the detector plane, illustrating the double-focusing properties of the Mattauch-Herzog geometry and the ability to resolve a spatially distributed pattern of ions passed through the system in first order. Note that the pattern flips during its passage through the magnetic sector. (Color Online)

in Figure 4a and b, along with some characteristic particle trajectories from the simulation platform shown in Figure 4c.

The initial distribution of particles shown in Figure 5a pass through the electric and magnetic fields generated in COMSOL Figure 4a and b and produce the ion distribution shown in Figure 5b. Comparing the simulated detector output from the transfer matrix method in Figure 2b and the COMSOL/C# simulation, we see that the predicted demagnification of the pattern is not as substantial in the COMSOL/C# simulation as in the transfer matrix method. Additionally, there is a non-uniform distortion across the pattern that was not present in the transfer matrix method pattern. These effects are likely due to the fringing fields at the entrance and exit of the electric sector, which were not accounted for in the results presented in Figure 2. This mild pattern distortion can be readily accounted for in the forward model of the system used in the deconvolution and reconstruction of the coded aperture spectra, as previously described in detail and shown experimentally [1, 2].

Experimental Verification of Spatial Aperture Coding in the Mattauch-Herzog Geometry

Experimental validation of the compatibility of spatial aperture coding with the Mattauch-Herzog geometry is demonstrated here using the commercially available OI Analytical/Xylem IonCam Transportable Mass Spectrometer miniature

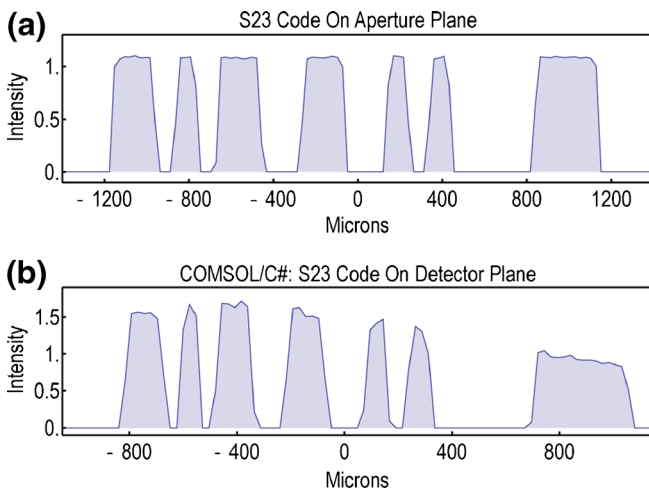


Figure 5. (a) Initial ion distribution across the object plane to be passed through the particle tracing simulation. (b) Expected ion distribution on the detector plane for Ar^{+1} ($40 m/z$) after passing through the particle tracing simulation. One million ions were simulated with an energy of 800 ± 8 eV from a point source 4 cm behind the aperture and a bin size of $24 \mu\text{m}$ was used for plotting the histograms. We observe the coded aperture pattern experiences a small demagnification and a non-uniform distortion across its expanse, but remains clearly resolvable on a detector with $24 \mu\text{m}$ pitch spacing, such as the one used for the experimental portion of this work [31]

Mattauch-Herzog mass spectrograph (OI Analytical, a Xylem brand, College Station TX, USA). The mass resolution for this spectrograph is cited as 24 at $6 m/z$ and 250 at $250 m/z$ [34]. The ion source for this system is a dual tungsten filament Nier-type [35] electron ionization source. The stock object slit in the system was replaced by a microfabricated spatially coded aperture (such as those described in [1, 2]) with minimum slit width of $100 \mu\text{m}$. Although the simulations presented in this work show promising results for apertures up to order S-23, the dimensions of the electric sector gap in the mass spectrograph used here allowed apertures only as large as an S-7 aperture pattern (with expected improvement in signal intensity of $4\times$).

Experimental results from the S-7 aperture are shown in Figure 6d. Transfer matrix and particle tracing results for this pattern are also shown in Figure 6b and c. For this smaller pattern, we see the same results as above for the transfer matrix and particle tracing methods. The experimental results show a demagnification similar to that of the particle tracing method, but the resolution is slightly worse than predicted, and there is an intensity drop off at the edges of the pattern. These effects of non-uniform intensity are attributed to the following: (i) the stock ion source not uniformly illuminating the spatial expanse of the coded aperture, (ii) effects resulting from the narrow electric sector gap, and (iii) non-uniform attenuation of the pattern intensity by the round Herzog-style shunts positioned at the entrance and exit of the electric sector gap. The reduction in resolution could be the result of small misalignments of the

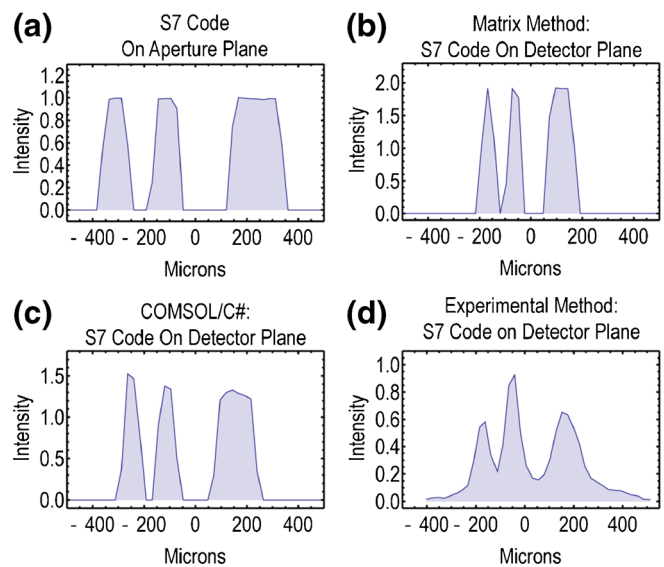


Figure 6. (a) Initial ion distribution across the object plane to be passed into the simulations. (b) Expected ion distribution on the detector plane based on transfer matrix models of the system. (c) Expected ion distribution on the detector plane based on particle tracing models of the system. (d) Experimentally measured ion distribution of Ar^{+1} (m/z 40) peak for an S-7 spatially coded aperture incorporated into the miniature Mattauch-Herzog type mass spectrograph commercially available from OI Analytical/Xylem (OI Analytical a Xylem brand, College Station TX)

detector plane or object aperture plane from the ideal focal planes of the system. Although an image of the S-7 code was observed on the detector demonstrating the compatibility of the MHMS with aperture coding, the non-uniform intensity profile along with the reduction of resolution prevented an accurate spectral reconstruction from the data. Optimizing the system by making the changes suggested above should allow for an accurate spectral reconstruction and are the subject of future work.

Conclusions

We have demonstrated the first application of spatial aperture coding to the Mattauch-Herzog mass spectrograph through (1) first principles transfer matrix calculations, (2) high fidelity particle tracing, and (3) experimentally using a commercially available miniature Mattauch-Herzog mass spectrograph. The first principles transfer matrix approach showed exceptional pattern mapping and indicated compatibility of this instrument geometry with spatial aperture coding. The high fidelity particle tracing method verified the results of the transfer matrix method, and indicated a non-uniform distortion of larger spatially distributed patterns because of off-axis effects that can be improved upon by new sector designs in future work. The simulations of the MHMS geometry indicate that close to the theoretical throughput of coded apertures up to order S-23 would be expected with a system designed to accept the dimensions of these codes. This compares favorably with the experimental results obtained from the simple magnetic sector published previously [1, 2]. An S-7 aperture was successfully imaged experimentally on a commercially available miniature MHMS. However, spectral reconstruction was not possible because of aberrations in the image that are a result of the experimental apparatus not being optimized for coded apertures. Based on the simulation results and successful imaging of a coded aperture experimentally, the MHMS is expected to provide improved throughput and resolution compared with the magnetic sector in [1, 2] attributable to the minimization of dispersions in the ion energy and angles, but this will not be demonstrable until an experimental system with the geometric modifications are available for an MHMS geometry as described in the experimental verification section. New sector designs that improve the image transfer of the spatially coded apertures along the mass dispersive dimension of this geometry to correct for these distortions will be the subject of future work. The order of magnitude gains in signal intensity shown in the transfer matrix and high fidelity particle tracing simulations are expected to be obtainable experimentally after hardware modifications that increase the electric sector gap. This work describes the application of coded aperture mass spectrometry to a double-focusing instrument, the Mattauch-Herzog. By increasing the sensitivity for a given resolution through the use of coded apertures, the MHMS is expected to become viable for miniaturized applications.

Acknowledgments

The authors acknowledge that this work was sponsored in part by a contract with the Department of Homeland Security Science and Technology Directorate.

References

1. Chen, E.X., Russell, Z.E., Amsden, J.J., Wolter, S.D., Danell, R.M., Parker, C.B., Stoner, B.R., Gehm, M.E., Glass, J.T., Brady, D.J.: Order of magnitude signal gain in magnetic sector mass spectrometry via aperture coding. *J. Am. Soc. Mass Spectrom.* **26**, 1633–1640 (2015)
2. Russell, Z.E., Chen, E.X., Amsden, J.J., Wolter, S.D., Danell, R.M., Parker, C.B., Stoner, B.R., Gehm, M.E., Brady, D.J., Glass, J.T.: Two-dimensional aperture coding for magnetic sector mass spectrometry. *J. Am. Soc. Mass Spectrom.* **26**, 248–256 (2015)
3. McLuckey, S.A., Wells, J.M.: Mass analysis at the advent of the 21st century. *Chem. Rev.* **101**, 571–606 (2001)
4. McLafferty, F.W.: A century of progress in molecular mass spectrometry. *Annu. Rev. Anal. Chem.* **4**, 1–22 (2011)
5. Bencsath, F.A., Plakas, S.M., Long, A.R.: Optimization of the analytical performance of the magnetic-sector mass-spectrometer for the identification of residual chloramphenicol in shrimp. *Biol. Mass Spectrom.* **23**, 665–674 (1994)
6. Takats, Z., Cotte-Rodriguez, I., Talaty, N., Chen, H.W., Cooks, R.G.: Direct, trace level detection of explosives on ambient surfaces by desorption electrospray ionization mass spectrometry. *Chem. Commun.* **15**, 1950–1952 (2005)
7. Forbes, T.P., Sisco, E.: Mass spectrometry detection and imaging of inorganic and organic explosive device signatures using desorption electro-flow focusing ionization. *Anal. Chem.* **86**, 7788–7797 (2014)
8. Hoffman, J.H., Hodges, R.R., Duerksen, K.D.: Pioneer Venus large probe neutral mass-spectrometer. *J. Vac. Sci. Technol.* **16**, 692–694 (1979)
9. Hoffmann, H.J., Pelka, K., Vonzahn, U., Krankowsky, D., Linkert, D.: The Pioneer Venus bus neutral gas mass-spectrometer. *IEEE Trans. Geosci. Remote* **18**, 122–126 (1980)
10. Nier, A.O., Hayden, J.L.: A miniature Mattauch-Herzog mass spectrometer for the investigation of planetary atmospheres. *Int. J. Mass Spectrom. Ion Phys.* **6**, 339–346 (1971)
11. Bell, R.J., Davey, N.G., Martinsen, M., Collin-Hansen, C., Krogh, E.T., Gill, C.G.: A field-portable membrane introduction mass spectrometer for real-time quantitation and spatial mapping of atmospheric and aqueous contaminants. *J. Am. Soc. Mass Spectrom.* **26**, 212–223 (2015)
12. Albaiges, J., Albrecht, P.: Fingerprinting marine pollutant hydrocarbons by computerized gas chromatography-mass spectrometry. *Int. J. Environ. Anal. Chem.* **6**, 171–190 (1979)
13. Jarmusch, A.K., Pirro, V., Kerian, K.S., Cooks, R.G.: Detection of strep throat causing bacterium directly from medical swabs by touch spray-mass spectrometry. *Analyst* **139**, 4785–4789 (2014)
14. Chace, D.H.: Mass spectrometry-based diagnostics: the upcoming revolution in disease detection has already arrived. *Clin. Chem.* **49**, 1227–1228 (2003)
15. Diaz, J.A., Giese, C.F., Gentry, W.R.: Sub-miniature ExB sector-field mass spectrometer. *J. Am. Soc. Mass Spectrom.* **12**, 619–632 (2001)
16. Kogan, V.T., Pavlov, A.K., Chichagov, Y.V., Tuboltsev, Y.V., Gladkov, G.Y., Kazanskii, A.D., Nikolaev, V.A., Pavlichkova, R.: Design and testing of a portable magnetic mass spectrometer. *Field Anal. Chem. Technol.* **1**, 331–342 (1997)
17. Hemond, H.F., Mueller, A.V., Hemond, M.: Field testing of lake water chemistry with a portable and an AUV-based mass spectrometer. *J. Am. Soc. Mass Spectrom.* **19**, 1403–1410 (2008)
18. Badman, E.R., Cooks, R.G.: Special feature: perspective—miniature mass analyzers. *J. Mass Spectrom.* **35**, 659–671 (2000)
19. Brady, D.J.: *Optical Imaging and Spectroscopy*, pp. 333–486. John Wiley and Sons, Hoboken (2009)
20. Eckhardt, C.J., Gross, M.L.: A proposed technique for signal multiplexing in mass spectrometry. *Int. J. Mass Spectrom. Ion Phys.* **5**, 223–227 (1970)
21. Aston, F.W.: A Positive ray spectrograph. *Philos. Mag.* **38**, 707–714 (1919)
22. Harwit, M., Sloane, N.J.A.: *Hadamard Transform Optics*. Academic Press, Waltham (1979)
23. Golay, M.J.E.: Multi-slit spectrometry. *J. Opt. Soc. Am.* **39**, 437–444 (1949)

24. Mattauch, J., Herzog, R.: About a new mass spectrograph. *Z. Phys.* **89**, 786–795 (1934)
25. Bainbridge, K.T., Jordan, E.B.: Mass spectrum analysis 1. The mass spectrograph 2. The existence of isobars of adjacent elements. *Phys. Rev.* **50**, 282–296 (1936)
26. Hintenberger, H., König, L.A.: Mass spectrometers and mass spectrographs corrected for image defects. In: Waldron, J.D. (ed.) *Advances in Mass Spectrometry*, pp. 16–35. Pergamon Press Ltd, London (1959)
27. Burgoyne, T.W., Hiefje, G.M.: An introduction to ion optics for the mass spectrograph. *Mass Spectrom. Rev.* **15**, 241–259 (1996)
28. Wollnik, H., Berz, M.: Relations between elements of transfer-matrices due to the condition of symplecticity. *Nucl. Instrum. Methods A* **238**, 127–140 (1985)
29. Wollnik, H.: *Optics of Charged Particles*. Academic Press, San Diego (1987)
30. Herzberger, M.: *Modern Geometrical Optics* (reprint edition 1980 with corrections). Krieger Publishing Company, Malabar (1980)
31. Hadjar, O., Johnson, G., Laskin, J., Kibelka, G., Shill, S., Kuhn, K., Cameron, C., Kassan, S.: IonCCD (TM) for direct position-sensitive charged-particle detection: from electrons and keV ions to hyperthermal biomolecular ions. *J. Am. Soc. Mass Spectrom.* **22**, 612–623 (2011)
32. Hadjar, O., Fowler, W.K., Kibelka, G., Schnute, W.C.: Preliminary demonstration of an IonCCD as an alternative pixelated anode for direct MCP readout in a compact MS-based detector. *J. Am. Soc. Mass Spectrom.* **23**, 418–424 (2012)
33. Swope, W.C., Andersen, H.C., Berens, P.H., Wilson, K.R.: A computer-simulation method for the calculation of equilibrium-constants for the formation of physical clusters of molecules—application to small water clusters. *J. Chem. Phys.* **76**, 637–649 (1982)
34. OI Analytical. IonCam Transportable Mass Spectrometer Gas Chromatograph/Mass Spectrometer. Available at: <http://www.oico.com/documentlibrary/3390spec.pdf>. Accessed December 12 (2015)
35. Nier, A.O.: A mass spectrometer for routine isotope abundance measurements. *Rev. Sci. Instrum.* **11**, 212–216 (1940)